International Journal of Nanomedicine

Dovepress
open access to scientific and medical research

Open Access Full Text Article

ORIGINAL RESEARCH

Confined growth of multiple gold nanorices in dual-mesoporous silica nanospheres for improved computed tomography imaging and photothermal therapy

This article was published in the following Dove Medical Press journal:
International Journal of Nanomedicine

Limei Qin[1]
Dechao Niu[1]
Yu Jiang[1]
Jianping He[1]
Xiaobo Jia[1]
Wenru Zhao[1]
Pei Li[2]
Yongsheng Li[1]

[1]Laboratory of Low-Dimensional Materials Chemistry, Key Laboratory for Ultrafine Materials of Ministry of Education, School of Materials Science and Engineering, East China University of Science and Technology, Shanghai 200237, China; [2]Department of Applied Biology and Chemical Technology, The Hong Kong Polytechnic University, Hong Kong, China

Introduction: In this work, we have developed a novel "confined-growth" strategy to synthesize PEGylated multiple gold nanorices-encapsulated dual-mesoporous silica nanospheres (designated as PEGylated MGNRs@DMSSs) containing both small mesopores (2.5 nm) in the shell and large mesopores (21.7 nm) in the core based on a well-established, seed-mediated growth method. The photothermal effect and CT imaging ability were also studied.

Methods: The nanoparticles were characterized by Fourier transform infrared (FT-IR) spectra, N_2 absorption isotherms, Field-emission scanning electron microscopy (FE-SEM), Transmission electron microscopy (TEM), Inductively coupled plasma atomic emission spectroscopy (ICP-AES) and Confocal microscopy.

Results: The longitudinally-localized surface (LSPR) absorption properties of MGNRs@DMSSs can be easily tuned by altering the amount of $HAuCl_4$ in the gold growth solution. Additionally, the resultant PEGylated MGNRs@DMSSs have monodispersed, spherical morphology and good colloidal stability in an aqueous solution. More importantly, when exposed to NIR irradiation, the PEGylated MGNRs@DMSSs exhibit both higher temperature increments and better photothermal effects than that of single PEGylated gold nanorods at nearly an equivalent LSPR absorption. In addition, as CT contrast agents, the PEGylated MGNRs@DMSSs display a better CT imaging performance, in comparison with single PEGylated gold nanorods at the same Au concentration.

Conclusion: Taken together, results indicate the potential for MGNRs@DMSSs used in CT imaging-guided photothermal therapy. Such a simple "confined-growth" strategy within a porous matrix offers a promising platform to design and prepare novel metal(s) oxide@silica nanocomposites for use in further cancer bio-imaging and therapy.

Keywords: gold nanorices, dual-mesoporous silica, confined growth, imaging, photothermal effect

Introduction

Gold nanorods or nanorices (GNRs) with favorable localized surface plasmon resonance (LSPR) optical absorption within the range of the near-infrared (NIR) window (650–900 nm) allow to deeply penetrate living tissue with minimal invasiveness.[1] Due to its excellent optical properties, GNRs have been widely used in a range of biomedical applications, including light scattering imaging,[2] two-photon fluorescence imaging,[3] photoacoustic imaging (PA),[4,5] surface-enhanced Raman scattering imaging,[6] optical coherent tomography,[7] photothermal/photodynamic therapy,[8–10] and drug/gene delivery.[11] Until now, various methods have been reported for GNR synthesis, including electrochemical reduction,[12] seed-mediated growth,[13] photochemical reduction,[14] and

Correspondence: Dechao Niu; Yongsheng Li
Laboratory of Low-Dimensional Materials Chemistry, Key Laboratory for Ultrafine Materials of Ministry of Education, School of Materials Science and Engineering, East China University of Science and Technology, No 130, Meilong Road, Shanghai 200237, China
Email dcniu@ecust.edu.cn; ysli@ecust.edu.cn

submit your manuscript | www.dovepress.com
Dovepress
http://dx.doi.org/10.2147/IJN.S184192

microwave-assisted reduction.[15] However, most of these synthetic routes involve cationic surfactants cetyltrimethylammonium bromide (CTAB) as stabilizing agents, which can induce serious toxicity to cells and living tissues.[16,17] Moreover, it has been observed that GNRs are frequently aggregated under complex physiological environment, suggesting that their desirable and optimal functionality may be unachievable.[18]

To simultaneously improve the biocompatibility and structural stability of GNRs, various surface modifications have been attempted, including thiol-mediated CTAB displacement,[19] electrostatic adsorption,[20,21] ligand exchange,[22] and silica coating.[23–29] Among these strategies, silica or mesoporous silica exhibits promising prospects as coating materials to stabilize and develop more bio-friendly GNRs@silica nanocomposites. In addition, these GNRs@silica nanoparticles displayed great potential in cancer imaging and therapy due to their ease in surface modification, excellent biocompatibility, and high chemical and thermal stability. For example, Nie et al[27] developed GNRs embedded in large-pore mesoporous organosilica, which have a potential for the treatment of triple-negative breast cancer. Recently, Lee et al[28] reported the synthesis of the rabies virus-inspired silica-coated GNRs and their applications in the treatment of brain tumors through the neuronal pathway bypassing the blood–brain barrier. Li et al[29] designed and developed a novel kind of light-responsive biodegradable perfluoropentane-filled and mesoporous-silica-coated GNR nanorattles for enhanced ultrasound imaging/photoacoustic imaging dual-modality imaging-guided photothermal therapy of melanoma. In these systems, silica or mesoporous silica coating not only improved GNR structural stability but also endowed the nanocomposites with good biological properties. Unfortunately, most of the reported work on the synthesis of GNRs@silica nanocomposites involved a two-step process including the preparation of "pre-formed" GNRs and subsequent silica coating process, which led to difficulties in adjusting the resulting LSPR absorption properties. Moreover, only a few of GNRs have been loaded into the silica framework; thus, a larger number of silica components would be needed to produce the necessary LSPR properties.[26,27] To date, there are few reports on the synthesis and biological performance of the aggregated multiple GNRs in a nanoscale matrix. Therefore, it is highly desirable to develop a new approach to synthesize multiple GNR-loaded nanocomposites and to explore the relationship between their aggregating structure and biological performance.

Herein, we report a simple and efficient "confined growth" synthetic route for the fabrication of multiple GNR-encapsulated porous silica nanoparticles by employing core-shell-structured, dual-mesoporous silica spheres (DMSSs) as a nanoreactor. Due to the spatial confinement presented by their unique dual-mesoporous channels, gold (Au) seeds with an average diameter of 2–3 nm were absorbed and grown directly on GNRs only in the large pore channels of DMSSs without any further pore modification through a well-known seed-mediated growth pathway. In addition, the optical properties of multiple GNR-loaded DMSSs were easily tuned by controlling the amount of the Au precursor $HAuCl_4$ in the growth solution. To improve the nanocomposite biocompatibility, PEG molecules were covalently grafted onto the outer surface of the silica-based nanoparticles, resulting in the final formation of PEG-modified multiple GNRs encapsulated DMSSs (designated as PEGylated MGNRs@DMSSs). More importantly, when used as an imaging contrast or therapeutic agent, the PEGylated MGNRs@DMSSs had distinct advantages over the traditional single GNR-loaded silica nanoparticles: 1) the PEGylated MGNRs@DMSSs exhibited better photothermal properties with a larger temperature increment and enhanced cytotoxicity under NIR irradiation, compared with PEGylated GNRs with similar UV absorption peaks. 2) As a CT contrast agent, the PEGylated MGNRs@DMSSs displayed higher HU values than that of individual PEGylated GNRs at the same Au concentration.

Materials and methods

Reagents

Tetrahydrofuran (THF, analytical reagent), ammonia solution (NH_4OH, AR), hexadecyltrimethylammonium bromide (CTAB, 99%), fluorescein isothiocyanate (FITC), and 3-aminopropyl triethoxysilane (APTES) were all purchased from Aladdin (Shanghai, China). Hydrochloric acid (HCl, 36%–38%) and ethyl silicate (TEOS) were purchased from Lingfeng Chemical Reagent Co., Ltd, (Shanghai, China), and ethanol (AR) was purchased from Titan (Shanghai, China). Sodium borohydride ($NaBH_4$, 96%) was obtained from Tianlian Chemical Technology (Shanghai, China). Silver nitrate ($AgNO_3$, AR) was purchased from Shanghai Chemical Reagent Co. (Shanghai, China). l-Ascorbic acid (AA, AR), chloroauric acid ($HAuCl_4{\cdot}4H_2O$), and sulfuric acid (H_2SO_4, AR) were all obtained from Sinopharm Chemical Reagent Co. (Shanghai, China). mPEG-silane (MW 5,000 Da) and mPEG-SH (MW 5,000 Da) were purchased from Sigma-Aldrich Co. (St Louis, MO, USA). Ammonium nitrate (NH_4NO_3) was purchased from Hansi Chemical Industrial (Shanghai, China). Cell Counting Kit-8 (CCK-8) was obtained from Dojindo (Shanghai, China). RPMI-1640, PBS, FBS, immunol staining fix solution, calcein acetoxymethyl ester (calcein AM), propidium iodide (PI), and dilactate

(DAPI) were all obtained from KeyGEN BioTECH (Nanjing, China). All chemicals were used as received without further purification. Ultrapure water with a resistivity of ~18.2 MΩ cm was used as the solvent in all experiments.

Characterization

Fourier transform infrared (FT-IR) spectra were recorded on a Nicolet 5700 Thermo FT-IR spectrometer using the KBr wafer technique. N_2 absorption isotherms were measured at 77 K using a Micromeritics Tristar II 3020 system. The specific surface area and pore size distribution were calculated using Brunauer–Emmett–Teller (BET) and nonlocal density functional theory methods, respectively. Field-emission scanning electron microscopy (FE-SEM) images were obtained using a Hitachi S-4800 electron microscope. Transmission electron microscopy (TEM) observations were conducted on a JEOL-2100F electron microscope. Inductively coupled plasma atomic emission spectroscopy (ICP-AES) was employed to determine Au weight percentage. Confocal microscopy images were taken using a Fluoview FV1000 Confocal Microscope (Olympus Corporation, Tokyo, Japan).

Synthesis of DMSSs

Amphiphilic block copolymer PS_{131}-*b*-PAA_{16} was synthesized via sequential atomic transfer radical polymerization as described previously.[30] DMSSs were prepared according to the protocol previously reported from our group.[31] Briefly, 100 mg PS_{131}-*b*-PAA_{16} was first dissolved in 10 mL of THF. This was then poured into a solution containing 40 mL water, 100 mg CTAB, and 0.5 mL ammonia. The resulting mixture was then poured into 80 mL ethanol containing 323 µL TEOS. After stirring for 10 minutes, the solution was allowed to sit at room temperature for 18 hours. The products were then collected by centrifugation (9,000 rpm, 10 minutes) and washed with pure water. Removal of PS-*b*-PAA and CTAB was achieved in an ethanol solution containing 0.5 mL HCl at 80°C. The extracted products were thoroughly washed with THF to remove the PS-*b*-PAA, after which the as-prepared DMSSs were suspended in 5 mL pure water for later testing.

Synthesis of PEGylated MGNRs@DMSSs

The seed-mediated growth method was employed to synthesize PEGylated MGNRs@DMSSs.[23] First, Au seeds@DMSSs were prepared by chemical reduction of $HAuCl_4$ with $NaBH_4$. More specifically, 7.5 mL CTAB (0.1 M) was mixed with 0.25 mL $HAuCl_4$ (0.01 M) and 1 mL DMSSs (10 mg/mL). The final volume was adjusted to 9.4 mL by adding appropriate amount of pure water. Then 0.6 mL ice-cold $NaBH_4$ aqueous solution (0.01 M) was added to the above mixture, after which the color gradually changed from yellow to red. This color change indicated the successful formation of Au seeds@DMSSs. After aging for 2 hours, the samples were collected by centrifugation (4,000 rpm, 10 minutes), washed with pure water, and then resuspended in 1 mL pure water.

The MGNRs@DMSSs growth solution consisted of 80 mL CTAB (0.1 M), 4 mL $HAuCl_4$ (0.01 M), 0.64 mL $AgNO_3$ (0.01 M), 1.6 mL H_2SO_4 (0.5 M), and 0.64 mL ascorbic acid (0.1 M). Growth was initiated by adding 1 mL Au seeds@DMSSs and stopped after 20 hours by centrifugation (4,000 rpm, 10 minutes). The removal of CTAB was achieved using a 6 g L^{-1} NH_4NO_3 ethanol solution at 60°C for 12 hours. This incubation was performed twice to fully remove CTAB, after which MGNRs@DMSSs were resuspended in 1 mL pure water for subsequent use.

PEGylated MGNRs@DMSSs were prepared as described previously.[32] Briefly, 1 mL of the above MGNRs@DMSSs was diluted with 10 mL pure water and mixed with 1 mL mPEG-silane (0.012 M, MW =5,000 Da) in an aqueous solution at 70°C under vigorous stirring for 3 hours and for an additional 15 hours at room temperature. The products were then obtained after three successive washes with pure water.

Synthesis of individual PEGylated GNRs

As a control sample, individual GNRs were synthesized via seed-mediated growth method. Specifically, 7.5 mL CTAB (0.1 M) was mixed with 250 µL $HAuCl_4$ (0.01 M), and the final volume was adjusted to 9.4 mL by adding appropriate amount of pure water. Then 0.6 mL ice-cold $NaBH_4$ aqueous solution (0.01 M) was added to the above mixture, and Au seeds were formed immediately and were used within 2 hours. The GNR growth solution consisted of 80 mL CTAB (0.1 M), 4 mL $HAuCl_4$ (0.01 M), 0.54 mL $AgNO_3$ (0.01 M), 1.6 mL H_2SO_4 (0.5 M), and 640 µL ascorbic acid (0.1 M). Growth was initiated by adding 240 µL Au seeds solution and stopped after 20 hours by centrifugation (9,000 rpm, 10 minutes), and then dispersed in 5 mL pure water. For PEG surface modification, the CTAB-coated GNRs were stirred with 1 mL PEG-SH (30 mg/mL) overnight, and the final product (defined as individual PEGylated GNRs) was obtained.

Preparation of FITC-labeled PEGylated MGNRs@DMSSs

About 50 mg FITC was reacted with 500 µL (3-aminopropyl) triethoxysilane (APTES) in 5 mL ethanol for 24 hours in the dark.[33] Then, 100 µL FITC-APTES solution and 1 mL PEGylated MGNRs@DMSSs were added to 5 mL ethanol with shaking. This solution was then allowed to react

overnight in the dark. Finally, the resulting product was washed with ethanol and PBS several times before use.

In vitro photothermal ability of PEGylated MGNRs@DMSSs and their application in CT imaging

To investigate the photothermal effect induced by NIR plasmatic resonance, an aqueous solution (1 mL) containing PEGylated MGNRs@DMSSs and PEGylated GNRs (with an Au concentration of 70 μg/mL, respectively) and pure water were irradiated using an NIR laser (808 nm, 1.5 W, Hps3200; B&A Technology Co., Ltd, Shanghai, China) for 5 minutes. The temperature of the solution was measured using a digital thermometer with a thermocouple probe. The photothermal stability of the PEGylated MGNRs@DMSSs was analyzed by irradiating it with an 808 nm NIR laser for 5 minutes (laser ON), followed by natural cooling without NIR laser irradiation for 10 minutes (laser OFF). This cycle was repeated five times and then the UV-vis-NIR spectra of the irradiated samples were obtained to characterize the stability of their absorption properties.

In vitro CT contrast effect of the PEGylated MGNRs@DMSSs was investigated using a clinical CT system (SIEMENS Sensation 64). This was performed across a range of Au concentrations (0–5.3 mg/mL) and was then compared to PEGylated GNRs. Hounsfield unit (HU) values were obtained from the region of interest of each sample. Data analysis was performed by fitting to relaxivity and CT value curves using the OriginPro 9.0 program.

Confocal laser scanning microscopy (CLSM) analysis

The SMMC-7721 cell lines in the present work were purchased commercially from KeyGEN BioTECH. SMMC-7721 cells (human hepatoma cells, 10^4 cells per dish) were incubated in RPMI-1640 medium containing 10% FBS at 37°C for 24 hours. After incubation, the solution was replaced with fresh medium containing 50 μg mL^{-1} FITC-labeled PEGylated MGNRs@DMSSs and incubated for another 4 hours. The cells were then washed three times with PBS and incubated with DAPI for 10 minutes. Cells were then imaged with an excitation wavelength of 404 nm (for DAPI) and 488 nm (for FITC).

Cytotoxicity assay

Photothermal-induced cytotoxicity of PEGylated MGNRs@DMSSs was evaluated using SMMC-7721 cells. Briefly, SMMC-7721 cells (10^5 cells per well) were incubated in a humidified atmosphere containing 5% CO_2 at 37°C for 24 hours. Cells were then incubated with PEGylated nanoparticle suspensions (2.0 mL per well, 70 μg mL^{-1} Au concentration) for an additional 4 hours. After treatment, cells were exposed to an NIR laser (1.5 W cm^{-2}) for 5 minutes and stained with calcein AM and PI to explore the photothermal effect on cancer cells.

The cytotoxicity of both PEGylated MGNRs@DMSSs and PEGylated GNRs with or without NIR laser irradiation was performed by using CCK-8 assay. Briefly, SMMC-7721 cells (5×10^3 cells per well) were seeded in a 96-well plate and incubated at 37°C for 24 hours. After incubation, different amounts of the two suspensions (PEGylated MGNRs@DMSSs or GNRs, 0.1 mL per well, Au concentrations of 0, 8.75, 17.5, 35, or 70 μg mL^{-1}) were added to each well and incubated for an additional 4 hours. The cells were then irradiated using an NIR laser (1.5 W cm^{-2}) for 5 minutes. After 20 hours, the CCK-8 solution (10 μL) was added and the absorption at 450 nm was tested.

For flow cytometry assay, SMMC-7721 cells were planted at 5×10^4 cells/well in 96-well plates for 24 hours. Then the cells were subjected to various treatments: RPMI-1640, laser irradiation (5 minutes, 808 nm, 1.5 W/cm^2), PEGylated GNRs, PEGylated GNRs + laser (5 minutes, 808 nm, 1.5 W/cm^2), PEGylated MGNRs@DMSSs, PEGylated MGNRs@DMSSs + laser (5 minutes, 808 nm, 1.5 W/cm^2). The photothermal effect of PEGylated GNRs and PEGylated MGNRs@DMSSs was studied by flow cytometry.

In vivo photothermal ability and CT imaging

Female nude mice weighing 18–20 g were purchased from Shanghai SLAC Laboratory Animal Co. Ltd (Shanghai, China). All animal procedures were performed by following the protocols approved by the Institutional Committee for Animal Care and the policy of the National Ministry of Health.

To explore in vivo photothermal effects, 4-week-old female nude mice were injected subcutaneously on the right rear flank area with 5×10^6 SMMC-7721 cancer cells in 100 μL of serum-free RPMI-1640 medium. After xenografts reached about 5 mm in diameter, a PEGylated MGNRs@DMSSs solution ([Au]=5.3 mg/mL, 50 μL) was intratumorally injected into the tumor-bearing mice. The resulting temperature changes at the tumor site were then recorded using an infrared camera (Fotric 226) under 808 nm laser irradiation, and the images were conducted with AnalyzIR software.

For in vivo CT imaging, 100 µL PEGylated MGNRs@DMSSs solution ([Au]=5.3 mg/mL) was injected into normal female nude mice (4–6 weeks old, 18–20 g) via tail vein. Pre- and 10 minutes post-injection CT images of the liver were collected using a clinical CT imaging system (SIEMENS Sensation 64), and the HU values of the corresponding region were recorded.

In vivo systematic toxicity

Normal female nude mice (4–6 weeks old, 18–20 g) were injected with PEGylated MGNRs@DMSSs (100 µL, [Au]=5.3 mg mL-1). At 24 hours post injection, mice were sacrificed and all major organs (heart, liver, spleen, lungs, and kidneys) were harvested. Tissues were then sectioned and examined using H&E staining. Slides were examined with a NIKON Eclipse Ci optical microscope (NIKON Digital Sight DS-FI2; Nikon Corporation, Tokyo, Japan).

Results and discussion

Synthesis and characterization of PEGylated MGNRs@DMSSs

The detailed synthetic procedure for PEGylated MGNRs@DMSSs is illustrated in Scheme 1. First, DMSSs with small pores in the thin shell and large pores in the core were prepared using block copolymer polystyrene$_{131}$-*b*-poly (acrylic acid)$_{16}$ (PS$_{131}$-*b*-PAA$_{16}$) and cationic surfactant CTAB as dual templates according to our previously reported protocol.[31] TEM images (Figure S1A–D) and N_2 absorption results (Figure S2) show that the DMSSs have a well-defined spherical morphology and core-shell dual-mesoporous structure. Besides, DMSSs possess large mesopores of 21.7 nm in the core and small mesopores of 2.5 nm in the ultra-thin shell. In addition, the BET surface area and pore volume are 790.2 m^2/g and 1.35 cm^3/g, respectively. Second, due to the spatial confinement effect, both the generation of small Au seeds (2–3 nm) and their growth occurred only in the large pores of DMSSs. This nucleation growth can occur without any additional pore channel modification (eg, amino or thiol groups). In general, the successful Au loading in the pore channels is based on the electrostatic interaction between positively charged CTAB molecules located on the Au seeds and the negatively charged Si-OH groups of the inner pore surface of the silica. In a control experiment, no GNRs were observed in the interior of the nanospheres without CTAB in seed solution. Under these conditions, nanostar-like Au particles were located outside the DMSSs after the growth process (Figure S3). Finally, to improve biocompatibility and water dispersity, PEG molecules were grafted onto the surface of MGNRs@DMSSs via a condensation reaction between the PEG-silane and silicon-hydroxyl groups, thereby leading to the formation of the PEGylated MGNRs@DMSSs.

As shown in Figure 1A and B, ultra-small Au nanoparticles with an average diameter of 2.5 nm are observed in the large pore channels of the DMSSs, indicating that the formation of Au seeds occurred only in large rather than small pore channels. After the in situ Au growth process, the well-defined spherical morphology, good monodispersity, and dual-mesoporous structure of the silica nanoparticles were maintained (Figure 1C and D). The dark-field TEM image and corresponding energy dispersive spectroscopy (EDS) elemental mapping results (Figure 1E and F_1–F_3) of MGNRs@DMSSs show the distributions of various elements of O, Si, and Au, further indicating the successful loading of multiple GNRs into the DMSSs. Scanning electron microscopy (SEM) was employed to verify the position of GNRs. Results show that all of these GNRs are located in the interior, rather than exterior surface of the DMSS nanospheres (Figure S4). More importantly, multiple GNRs with an average aspect ratio of 3.75 were encapsulated in the large pore channels of the DMSSs. In addition, using an equivalent Au concentration in growth solution, CTAB-coated GNRs with a slightly larger average aspect ratio (4) were obtained in the absence of DMSSs (Figure S5A and B), indicating the spatial confinement effect of the large pores in DMSSs.

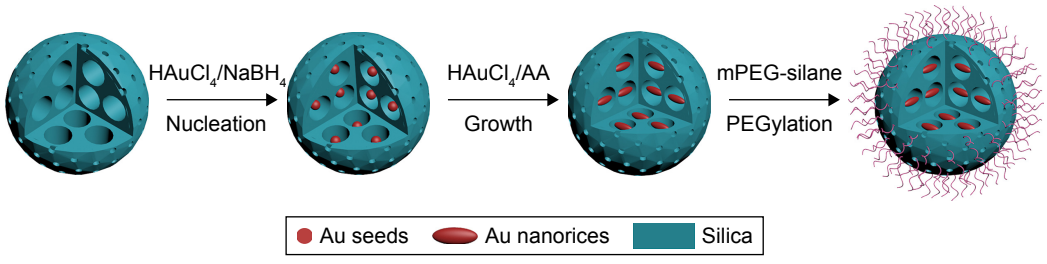

Scheme 1 Schematic illustration for the synthesis of PEGylated MGNRs@DMSSs.
Abbreviations: $HAuCl_4$, chloroauric acid; $NaBH_4$, sodium borohydride; AA, ascorbic acid; mPEG-silane, methoxyl silane functionalized polyethylene glycol; PEGylated MGNRs@DMSSs, mPEG-silane (Mw =5,000) modified multiple gold nanorices in dual-mesoporous silica nanospheres.

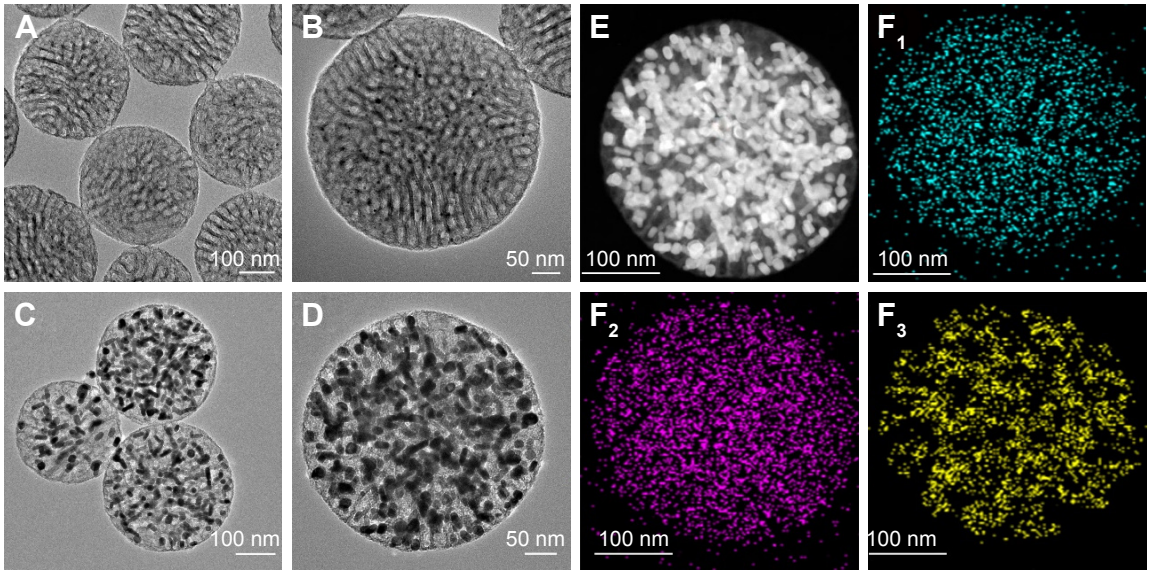

Figure 1 TEM images of Au seeds@DMSSs (**A**, **B**), MGNRs@DMSSs (**C**, **D**) at different magnifications. STEM images of MGNRs@DMSSs under dark field (**E**) and corresponding EDS elemental mapping of overlap O ($\mathbf{F}_1$), Si ($\mathbf{F}_2$) and Au ($\mathbf{F}_3$) in a single nanosphere.
Abbreviations: TEM, transmission electron microscopy; Au seeds@DMSSs, gold seeds encapsulated dual-mesoporous silica nanospheres; MGNRs@DMSSs, extracted multiple gold nanorices in dual-mesoporous silica nanospheres; STEM, scanning transmission electron microscopy; EDS, energy dispersive spectroscopy.

To characterize the improved structural stability of multiple GNRs in the DMSSs, both the as-prepared MGNRs@DMSSs without CTAB removal and the CTAB-coated GNRs were subjected to the extraction process. This process required exposure to an EtOH/NH_4NO_3 solution at high temperature (~60°C). As shown in Figure S5C and D, the as-prepared MGNRs@DMSSs exhibit a stable and well-dispersed black-red-colored solution after the extraction process. In contrast, CTAB-coated GNRs precipitated from an initial black-brown solution to yellow sticky solid. This indicates that the structural stability of GNRs could be protected and improved by the spatial confinement effect in the pore channels of the DMSSs.

One of the intrinsic advantages of the in situ seed growth method is the ability to control the GNR growth (Au amounts) by varying the composition of the growth solution itself. In the present work, four samples (designated as MGNRs@DMSSs-2.5, MGNRs@DMSSs-3, MGNRs@DMSSs-4, and MGNRs@DMSSs-5) were prepared by using different growth solutions containing varied volumes $HAuCl_4$ (2.5, 3, 4, and 5 mL) to adjust GNR growth to fill the large pores of the DMSSs. As shown in Figure 2, all four samples exhibit a spherical morphology and a number of GNRs are located in the interior of the large pore channels of the DMSSs. More importantly, when the volume of $HAuCl_4$ in the growth solution increased from 2.5 to 5 mL, the average GNR aspect ratios in the DMSSs increased from 3.26 to 3.86. Accordingly, the maximum NIR absorption wavelength of MGNRs@DMSSs red-shifted from 730 to 787 nm (Figure $2A_4$, B_4, and C_4). However, for the sample of MGNRs@DMSSs-5, part of particles exhibited non-spherical morphology and a few GNRs were found outside of the nanoparticles (Figure $2C_3$). It is probably attributed to the excessive growth of GNRs in the large pore channels. To highlight the importance of mesoporous silica, control samples without the mold (mesoporous silica) were prepared by using the equivalent amount of $HAuCl_4$ in the growth solution varying from 2.5 to 5 mL. Compared to the MGNRs@DMSSs, larger NIR adsorption peaks of GNRs varying from 761 to 798 nm can be obtained (Figure S6), demonstrating the confinement effect of mesoporous structures. In addition, to investigate the effect of the pore size on the growth of Au seeds in the pores, DMSSs-PS_{92} with large pore size of 12.7 nm were synthesized by using PS_{92}-*b*-PAA_{22} as pore template (Figure S7). After the growth of Au seeds in DMSSs-PS_{92} with equivalent amount of $HAuCl_4$, most of Au nanoparticles are rod-like, and not the rice-shaped particles. Moreover, there are a variety of GNRs located on the surface of DMSSs-PS_{92} (Figure S8). Thus, considering the structural integrity of the nanoparticles and the maximum absorption wavelength in the NIR region, we chose the sample of MGNRs@DMSSs-4 for subsequent PEG modification and biological testing.

As reported previously, the modification of the particle surface with PEG molecules is an effective strategy for improving biocompatibility and reducing phagocytic capture by the immune system.[34–36] Here, PEG molecules were

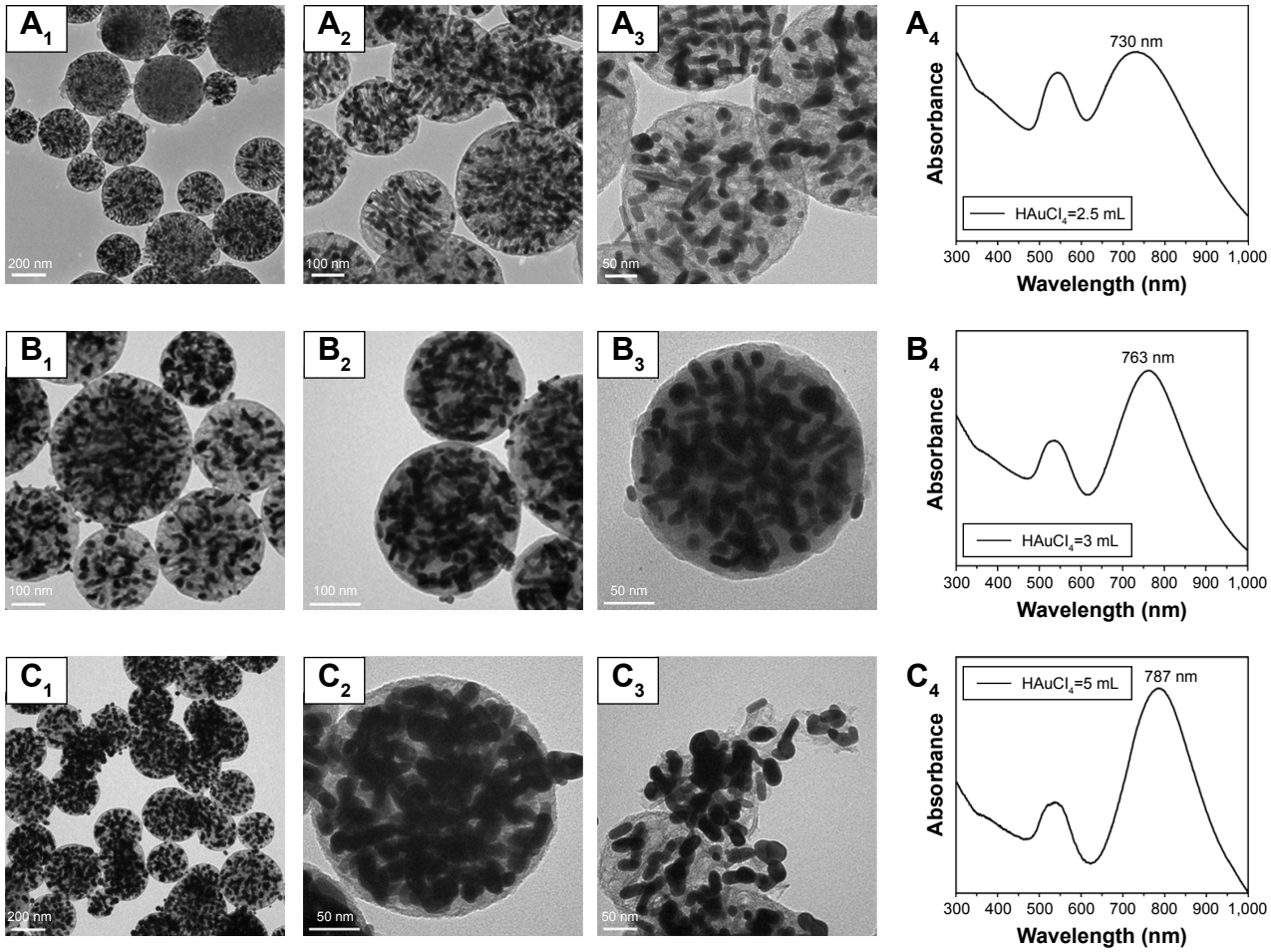

Figure 2 TEM images and corresponding UV-vis-NIR spectra of MGNRs@DMSSs prepared using different growth solutions in varying volumes of $HAuCl_4$: (**A_1**–**A_4**) 2.5 mL, (**B_1**–**B_4**) 3 mL, and (**C_1**–**C_4**) 5 mL.

Abbreviations: MGNRs@DMSSs, extracted multiple gold nanorices in dual-mesoporous silica nanospheres; UV, ultraviolet; NIR, near-infrared; TEM, transmission electron microscopy.

covalently grafted onto the outer surface of the DMSSs through silane chemistry. As shown in Figure 3A–C, both the spherical morphology of DMSS and its dual-mesoporous structure were maintained after PEGylation. To confirm the successful grafting of PEG, FT-IR spectra of the as-prepared MGNRs@DMSSs, MGNRs@DMSSs, and PEGylated MGNRs@DMSSs were recorded (Figure 3D). Compared to the MGNRs@DMSSs, PEGylated MGNRs@DMSSs show an absorption band at ~2,900 cm^{-1} belonging to the C–H groups of PEG, demonstrating the successful grafting of PEG onto the surface of MGNRs@DMSSs. The average hydrodynamic diameter of PEGylated MGNRs@DMSSs as measured by dynamic light scattering (Figure 3E) in water is ~340 nm, which is slightly larger than that obtained from TEM images of MGNRs@DMSSs. To demonstrate the colloidal stability in a biological environment, we measured the hydrodynamic diameter of the PEGylated MGNRs@DMSSs and MGNRs@DMSSs dispersed in RPMI-1640 with 10% calf serum. Results show that the dynamic diameter of PEGylated MGNRs@DMSSs was stable at ~340 nm for as long as 6 days (Figure 3F). In comparison, the particle size of extracted MGNRs@DMSSs increased to 440 nm over the same time range. This change in diameter likely originated from the nonspecific adsorption of medium-sized proteins, resulting in an increased particle size.[35,37] Besides, the final Au concentration of PEGylated MGNRs@DMSSs was determined to be 5.3 mg/mL using ICP-AES analysis.

Optical absorption and photothermal property of PEGylated MGNRs@DMSSs

Prior to evaluating the photothermal effect of the PEGylated MGNRs@DMSSs, the UV-vis spectra of samples obtained at different synthetic stages were recorded (Figure 3G). Results show that the Au seeds@DMSSs have a typical absorption peak at 518 nm, which could be attributed to the formation of spherical Au seeds after the reduction process.[38] After the

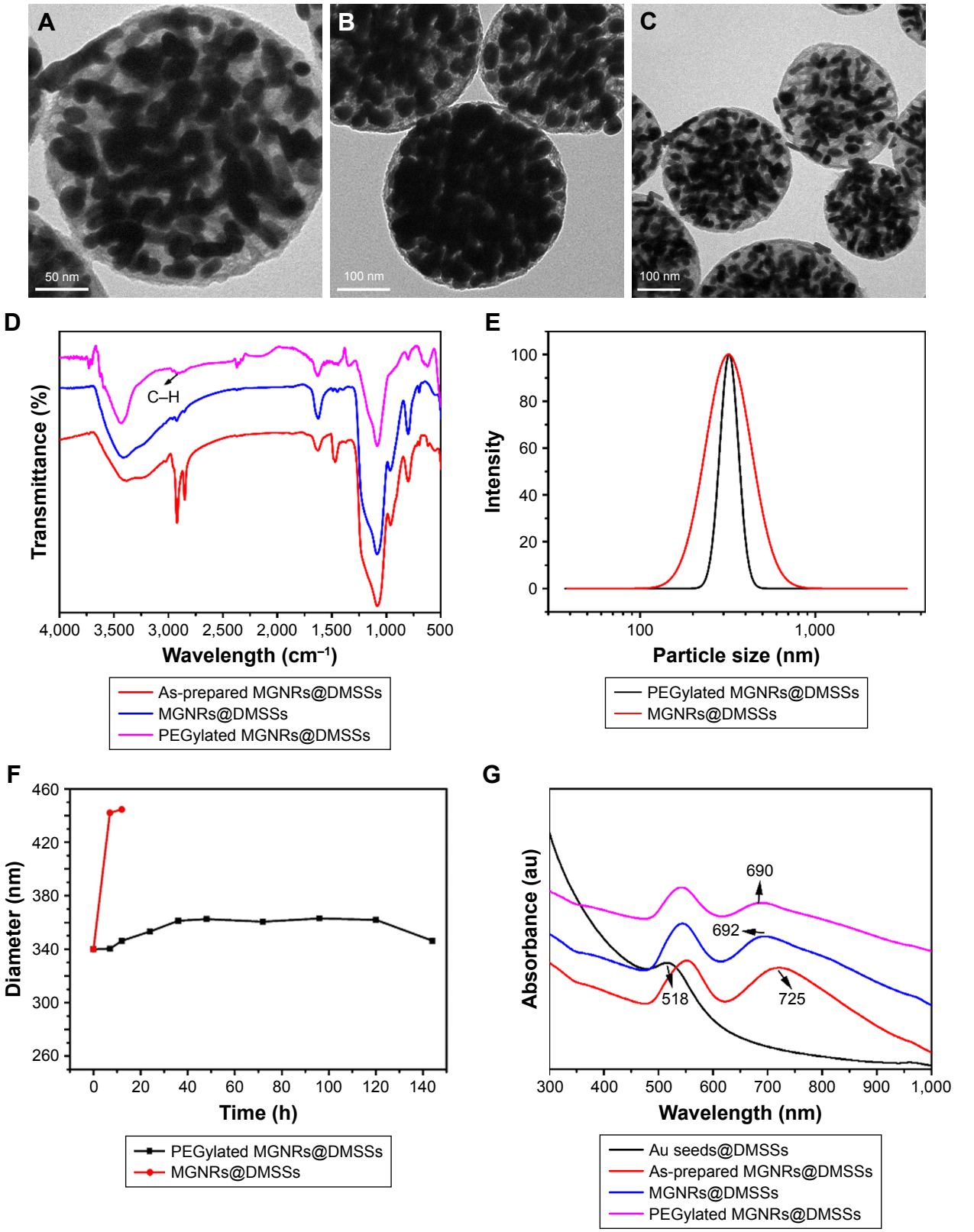

Figure 3 (**A**–**C**) TEM images of PEGylated MGNRs@DMSSs at different magnifications, (**D**) FT-IR spectra of as-prepared MGNRs@DMSSs, MGNRs@DMSSs, and PEGylated MGNRs@DMSSs. (**E**) Dynamic light scattering (DLS) of MGNRs@DMSSs and PEGylated MGNRs@DMSSs. (**F**) Long-term colloidal stability of MGNRs@DMSSs and PEGylated MGNRs@DMSSs in RMPI-1640 with 10% calf serum. (**G**) UV-vis-NIR spectra of Au Seeds@DMSSs, as-prepared MGNRs@DMSSs, MGNRs@DMSSs, and PEGylated MGNRs@DMSSs.

Abbreviations: TEM, transmission electron microscopy; PEGylated MGNRs@DMSSs, PEG-modified multiple gold nanorices in dual-mesoporous silica nanospheres; FT-IR, Fourier transform infrared spectroscopy; as-prepared MGNRs@DMSSs, as-prepared multiple gold nanorices in dual-mesoporous silica nanospheres; MGNRs@DMSSs, extracted multiple gold nanorices in dual-mesoporous silica nanospheres; Au Seeds@DMSSs, gold seeds encapsulated dual-mesoporous silica nanospheres.

growth of Au seeds, two notable absorption peaks centered at 530 and 725 nm are observed, along with a simultaneous color change of the solution from pink to purple, indicating the successful formation of GNRs. Compared to the as-prepared MGNRs@DMSSs, a 33 nm blue shift is found in the spectrum of the MGNRs@DMSSs. This is likely the result of slight distortions on the loaded GNRs caused by the high extraction temperatures.[39] Fortunately, PEGylation of the nanoparticles did not notably change the NIR absorbance peak since there was only a slight blue shift (2 nm) after PEG modification. As a result, the final absorption peaks of PEGylated MGNRs@DMSSs were 518 and 690 nm, which were still located within the NIR absorption range (650–900 nm).

It has been reported that the likelihood of hyperthermia-induced apoptosis increases substantially at temperatures ≥45°C.[13,40] In the present work, due to the aggregation behavior of multiple GNRs in DMSSs, it is necessary to explore the photothermal effect of PEGylated MGNRs@DMSSs. To investigate the in vitro photothermal ability, the temperature increment of PEGylated MGNRs@DMSSs was recorded using an 808 nm NIR laser irradiation. As shown in Figure 4A, after 5 minutes irradiation, the temperature of a PEGylated MGNRs@DMSSs solution containing Au concentrations of either 40, 80, or 160 μg/mL increased by 23.4, 26.7, and 30.3°C, respectively. In comparison, irradiated pure water only changed 1.4°C at the same condition. To evaluate the NIR photostability of PEGylated MGNRs@DMSSs, five laser ON/OFF cycles of NIR laser irradiation were tested (Figure 4B). A temperature increment of 30°C was achieved in the first cycle, and there was no significant temperature decrease after five cycles. In addition, there was no obvious blue shift in the LSPR band of PEGylated MGNRs@DMSSs after five laser ON/OFF cycles (Figure S9). These indicate that the silica framework is capable to protect GNRs from reshaping during NIR laser irradiation.[40]

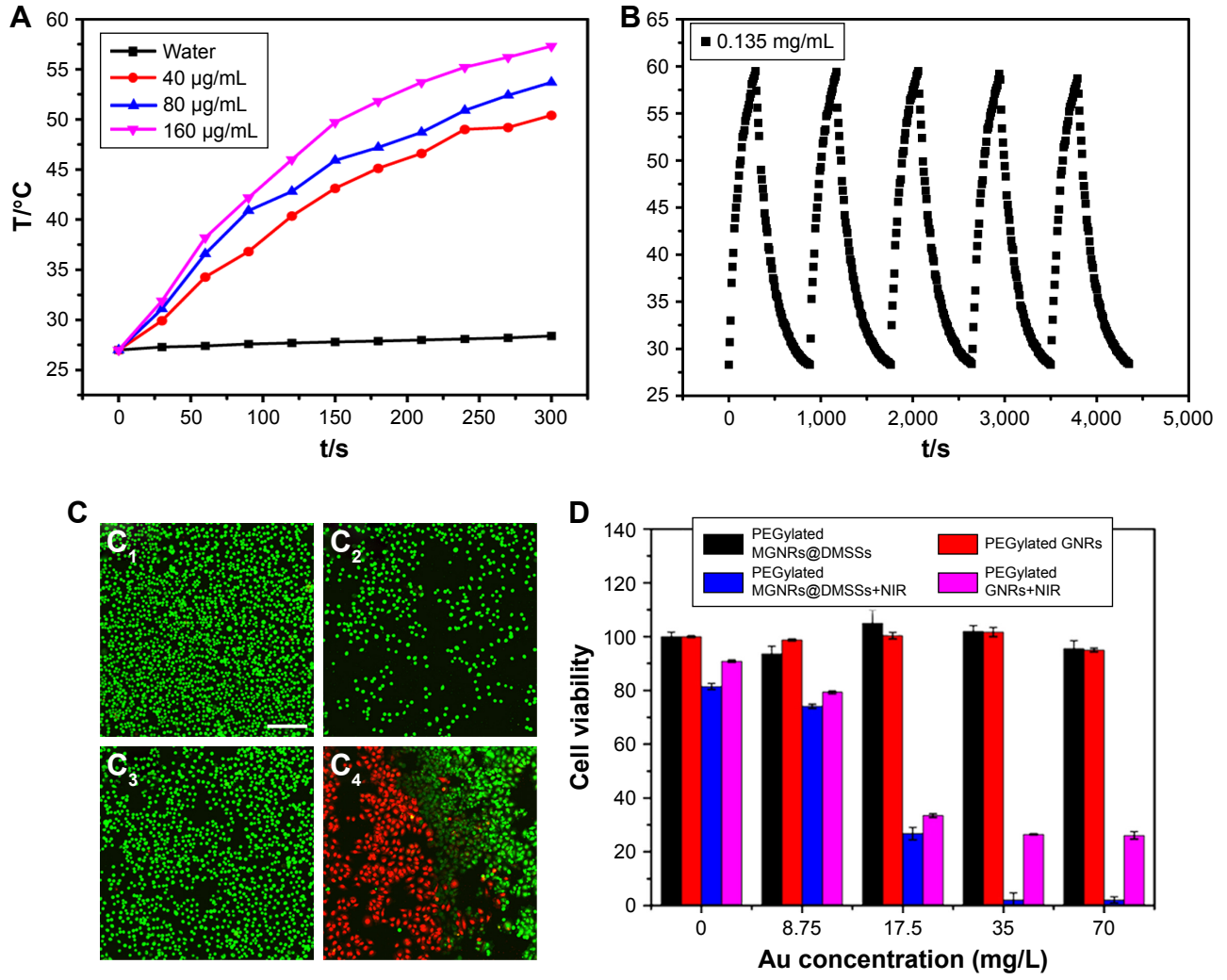

Figure 4 (*Continued*)

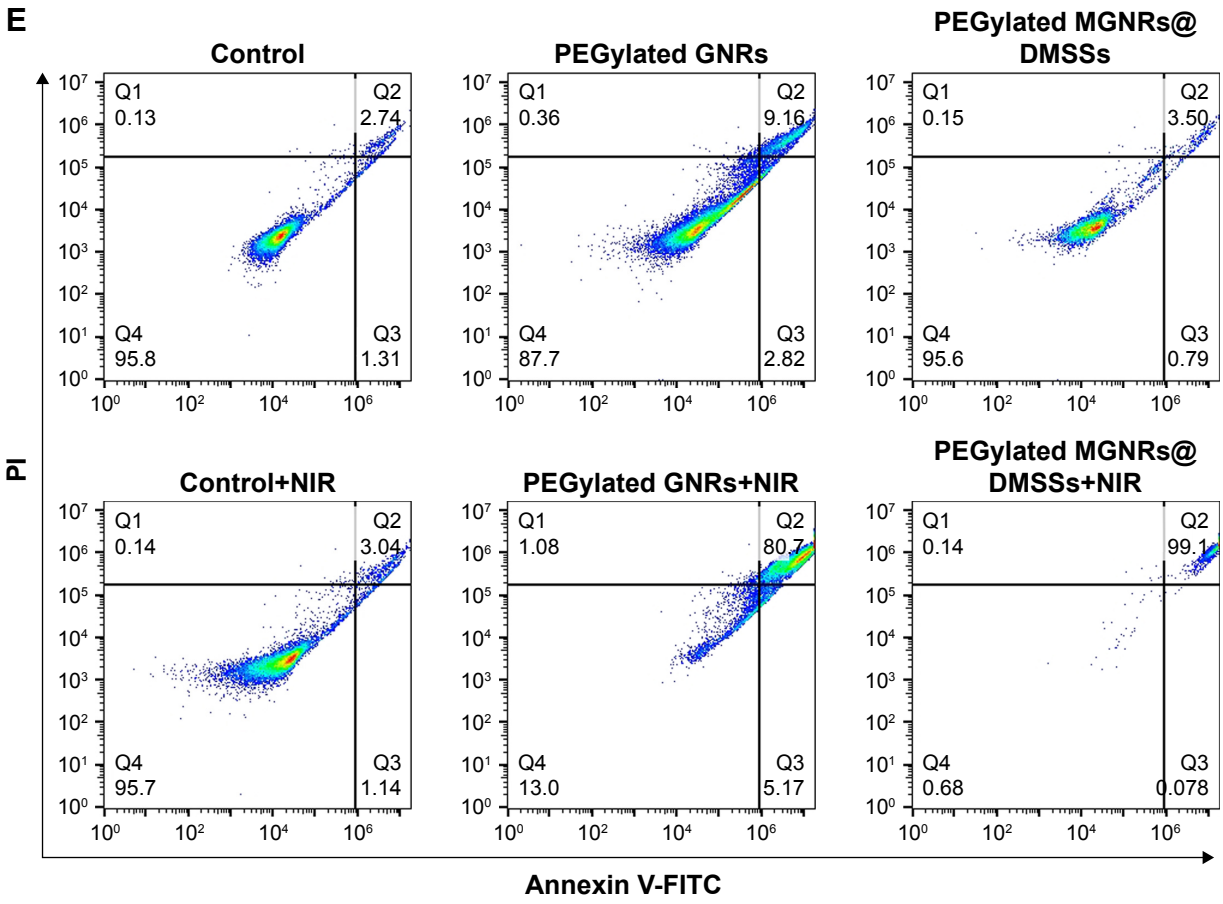

Figure 4 (**A**) Photothermal effect of PEGylated MGNRs@DMSSs aqueous solution at different Au concentrations with NIR laser irradiated (808 nm, 1.5 W cm^{-2}) for 5 minutes. (**B**) Photothermal stability of PEGylated MGNRs@DMSSs with Au concentration of 0.135 mg/mL during five cycles of 808 nm NIR laser irradiation (1.5 W/cm^2) for 300 seconds and cooling down for 600 seconds. (**C**) Confocal microscopic images of SMMC-7721 cells treated with different groups: (C_1) control group, (C_2) laser irradiation only, (C_3) PEGylated MGNRs@DMSSs only, and (C_4) PEGylated MGNRs@DMSSs with laser irradiation (all images were stained with calcein AM and PI, where green fluorescence from calcein AM and red fluorescence from PI indicate live and dead cells, respectively). Scale bars are 200 μm. (**D**) Relative cell viabilities of SMMC-7721 cells after 24 hours incubation with PEGylated MGNRs@DMSSs and PEGylated GNRs at different Au concentrations with or without laser irradiation. (**E**) Flow cell apoptosis of SMMC-7721 cells treated with different groups, where green fluorescence from Annexin V-FITC and red fluorescence from PI indicate live and dead cells, respectively.
Abbreviations: PEGylated MGNRs@DMSSs, mPEG-silane (Mw =5,000) modified multiple gold nanorices in dual-mesoporous silica nanospheres; NIR, near-infrared; AM, acetoxymethyl; PI, propidium iodide.

Furthermore, the photothermal effect of PEGylated MGNRs@DMSSs in cell level by choosing SMMC-7721 (human hepatoma cell line) as model cell was investigated. A clear demarcation line between dead (red) and live (green) cells is observed in CLSM images in the presence of both PEGylated MGNRs@DMSSs and NIR irradiation (Figure 4C_1–C_4). Comparatively, most of the cells were alive (green) in the control groups. These indicate that PEGylated MGNRs@DMSSs induced SMMC-7721 cell death only under NIR laser irradiation condition. In contrast, either PEGylated MGNRs@DMSSs itself or laser irradiation alone was unable to cause the cell death. To further confirm the cellular uptake of PEGylated MGNRs@DMSSs, FITC was grafted onto the silica-based nanoparticles. As shown in Figure S10, the emission wavelength of the FITC-labeled PEGylated MGNRs@DMSSs is about 520 nm, indicating the successful graft of green fluorescent FITC molecules on the nanoparticles. In addition, significant intracellular fluorescence including cytoplasmic green luminescence and nuclear blue luminescence on SMMC-7721 cells is revealed (Figure S11), indicating the successful cellular uptake of PEGylated MGNRs@DMSSs.

In vitro and in vivo photothermal effect

To examine the in vitro photothermal effect, the cell viability of SMMC-7721 cells treated with PEGylated MGNRs@DMSSs with or without laser irradiation was determined by using a quantitative CCK-8 assay. For better comparison, individual PEGylated GNRs (Figure S12) with the same NIR absorption as PEGylated MGNRs@DMSSs were prepared by adjusting the amounts of $AgNO_3$ in accordance with the previously published work.[38,42] As shown in Figure 4D, >95%

SMMC-7721 cells remained viable after being treated with only PEGylated MGNRs@DMSSs or PEGylated GNRs. This finding suggests that both PEGylated MGNRs@DMSSs and PEGylated GNRs have good cellular biocompatibility, even at Au concentrations of up to 70 μg mL^{-1}. In contrast, a cell survival ratio <3% was noted for the group simultaneously treated with PEGylated MGNRs@DMSSs and NIR laser irradiation at an Au concentration of 70 μg mL^{-1}. While group treated simultaneously with PEGylated GNRs and laser irradiation maintained cell survival rates of 28.7% at an Au concentration of 70 μg mL^{-1}, demonstrating that the PEGylated MGNRs@DMSSs exhibited stronger photothermal ability than PEGylated GNRs. To quantify the cell apoptosis/necrosis, flow cytometry was employed by using annexinV-FITC/PI dual staining method (Figure 4E). The results show that the PEGylated MGNRs@DMSSs plus laser irradiation group induced higher apoptosis/necrosis rate (99.34%) of SMMC-7721 cells than that (87%) of PEGylated GNRs plus laser irradiation.

To explain the above results, the temperature curves of PEGylated GNRs and PEGylated MGNRs@DMSSs in an aqueous solution under the same NIR laser irradiation conditions and varying Au concentrations were tested (Figure S13). It is found that the temperature of PEGylated MGNRs@DMSSs solution increased to 53°C, which was higher than that (47°C) of PEGylated GNRs solution after NIR laser irradiation for 5 minutes. In addition, the photothermal conversion efficiency (η) of PEGylated MGNRs@DMSSs is calculated to be 28.2% according to the reported method,[41] which is higher than that (22.5%) of individual PEGylated GNRs (Figures S14 and S15). Thus, the possible reason for the enhanced cytotoxicity is the higher temperature increment/photothermal conversion efficiency achieved by employing PEGylated MGNRs@DMSSs as cellular photoabsorbers.[42] To investigate the photothermal effect in vivo, the tumor region in a mouse xenograft model was intratumorally injected with PEGylated MGNRs@DMSSs and then irradiated using an 808 nm NIR laser for 5 minutes. As shown in Figure S16, the tumoral temperature increased from 32.3°C to 60.3°C, which is high enough to ablate tumors in vivo. This demonstrates that PEGylated MGNRs@DMSSs are more effective photoabsorbers for inducing tumor cell death under the NIR irradiation in cancer therapy.

In vitro and in vivo CT imaging

X-ray computed tomography (CT) is an imaging diagnostic technique based on X-ray absorption of different tissues. As clinically used CT contrast agents, small iodinated molecules generally experience rapid renal excretion and allow short imaging time, which promote the development Au-based CT contrast agents. Although the CT imaging effect of both Au nanoparticles and GNRs have been widely reported in recent years,[3] a specific investigation into the use of multiple GNRs in a nanoscale matrix in CT imaging remains relatively unknown. In the present work, we sought to confirm the CT imaging advantages of multiple GNRs in a nanoscale matrix. As shown in Figure 5A, both PEGylated individual GNRs and PEGylated MGNRs@DMSSs solution at the same Au concentration showed brighter CT signals with increasing Au concentrations. Interestingly, the HU values of PEGylated MGNRs@DMSSs were significantly higher than those of PEGylated GNRs at the same Au concentration (Figure 5B). This difference can be attributed to the increased Au density in the nanoscale range, resulting in more X-ray adsorption for the PEGylated MGNRs@DMSSs. For in vivo CT imaging, CT images of normal mouse liver were collected before and 10 minutes post-injection. As shown in Figure 5C and D, compared to the control group (before injection), the liver area (indicated by the black circle) became brighter after the injection of Au-based nanoparticles. This corresponded to an increase in average HU values from 49 to 67. To verify the in vivo biocompatibility and biosafety, H&E staining images of the lung, liver, heart, kidney, and spleen from mice injected with PEGylated MGNRs@DMSSs were collected (Figure 5E). Results show that no significant histological alterations were detected in any of the tested tissues. Consequently, these findings indicate the potential application of PEGylated MGNRs@DMSSs in CT imaging and imaging-guided photothermal therapy.

Conclusion

In summary, we have developed a facile "confined growth" approach for the synthesis of PEGylated multiple GNRs encapsulated dual-mesoporous silica nanospheres (PEGylated MGNRs@DMSSs) using dual-mesoporous silica nanospheres as a hard template. Based on the spatial confinement effect presented by the dual-mesoporous structure, the formation of Au seeds and their growth only occurred in large rather than small pore channels. In addition, the optical properties of MGNRs@DMSSs are easily tuned by changing the amount of Au precursor contained within the growth solution. The resulting PEGylated MGNRs@DMSSs had uniform particle size distribution, good colloidal stability, and negligible cytotoxicity at the tested concentration range. More importantly, compared to PEGylated individual GNRs,

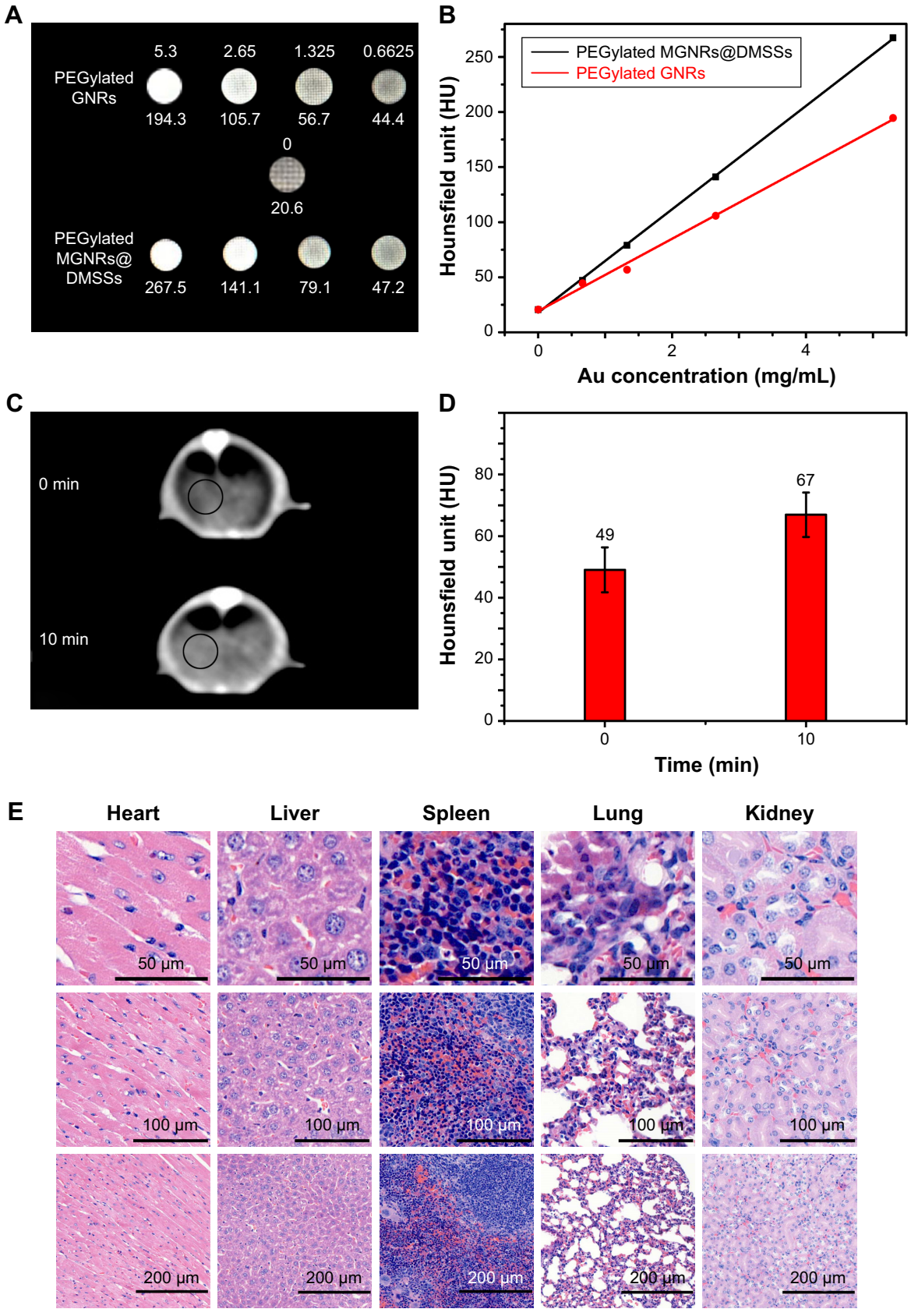

Figure 5 (**A**) CT scanning images and (**B**) corresponding CT attenuation plot of PEGylated MGNRs@DMSSs and PEGylated GNRs in varying Au concentrations in the range from 0 to 5.3 mg/mL. (**C**) In vivo CT images and (**D**) corresponding HU value of normal nude mice liver at 10 minutes post administration of PEGylated MGNRs@DMSSs (5.3 mg/mL, 100 μL). (**E**) Hematoxylin and eosin (H&E) stained images of major organs in nude mice treated with PEGylated MGNRs@DMSSs at 24 hours post-injection.
Abbreviations: CT, computed tomography; PEGylated MGNRs@DMSSs, PEG-modified multiple gold nanorices in dual-mesoporous silica nanospheres; PEGylated GNRs, PEGylated gold nanorods; HU, Hounsfield unit.

both the NIR adsorption photothermal effects and CT imaging capabilities of the PEGylated MGNRs@DMSSs were enhanced, which is likely due to the aggregation behavior of multiple GNRs in the large pore channels of the DMSSs. Consequently, these results highlight the potential use for PEGylated MGNRs@DMSSs as a theranostic nanoplatform for the CT diagnosis and treatment of solid tumors under NIR laser irradiation.

Acknowledgments

This work was financially supported by the National Natural Science Foundation of China for Innovative Research Groups (No 51621002); the National Key Research and Development Program of China (Grant No 2016YFA0203700); NSFC (Grant No 51572083, 51572084, 51461165202, and 51472085); Basic Research Program of Shanghai (17JC1404702); the Shanghai Rising-Star Program (16QA1401300); the Program for Professor of Special Appointment (Eastern Scholar) at Shanghai Institutions of Higher Learning, the 111 project (B14018); and The Fundamental Research Funds for Central Universities (222201718002).

Disclosure

The authors report no conflicts of interest in this work.

References

1. Pérez-Juste J, Pastorizasantos I, Lizmarzan L, Mulvaney P. Gold nanorods: synthesis, characterization and applications. *Coord Chem Rev*. 2005;249(17–18):1870–1901.
2. Huang X, El-Sayed IH, Qian W, El-Sayed MA. Cancer cell imaging and photothermal therapy in the near-infrared region by using gold nanorods. *J Am Chem Soc*. 2006;128(6):2115–2120.
3. Durr NJ, Larson T, Smith DK, et al. Two-photon luminescence imaging of cancer cells using molecularly targeted gold nanorods. *Nano Lett*. 2007;7(4):941–945.
4. Jia Q, Ge J, Liu W, et al. Gold nanorod@silica-carbon dots as multifunctional phototheranostics for fluorescence and photoacoustic imaging-guided synergistic photodynamic/photothermal therapy. *Nanoscale*. 2016;8(26):13067–13077.
5. Yang HW, Liu HL, Li ML, et al. Magnetic gold-nanorod/PNIPAAmMA nanoparticles for dual magnetic resonance and photoacoustic imaging and targeted photothermal therapy. *Biomaterials*. 2013;34(22):5651–5660.
6. Huang X, El-Sayed IH, Qian W, El-Sayed MA. Cancer cells assemble and align gold nanorods conjugated to antibodies to produce highly enhanced, SHARP, and polarized surface Raman spectra: a potential cancer diagnostic marker. *Nano Lett*. 2007;7(6):1591–1597.
7. Jung Y, Reif R, Zeng Y, Wang RK. Three-dimensional High-resolution imaging of gold nanorods uptake in sentinel lymph nodes. *Nano Lett*. 2011;11(7):2938–2943.
8. Liu J, Detrembleur C, de Pauw-Gillet MC, et al. Gold nanorods coated with mesoporous silica shell as drug delivery system for remote near infrared light-activated release and potential phototherapy. *Small*. 2015;11(19):2323–2332.
9. Zeng J-Y, Zhang M-K, Peng M-Y, Gong D, Zhang X-Z. Porphyrinic metal-organic frameworks coated gold nanorods as a versatile nanoplatform for combined Photodynamic/Photothermal/Chemotherapy of tumor. *Adv Funct Mater*. 2018;28(8):1705451.
10. Xu C, Chen F, Valdovinos HF, et al. Bacteria-like mesoporous silica-coated gold nanorods for positron emission tomography and photoacoustic imaging-guided chemo-photothermal combined therapy. *Biomaterials*. 2018;165:56–65.
11. Zhang Z, Wang J, Nie X, et al. Near infrared laser-induced targeted cancer therapy using thermoresponsive polymer encapsulated gold nanorods. *J Am Chem Soc*. 2014;136(20):7317–7326.
12. Chang S-S, Shih C-W, Chen C-D, Lai W-C, Wang CRC. The shape transition of gold nanorods. *Langmuir*. 1999;15(3):701–709.
13. Nikoobakht B, El-Sayed MA. Preparation and growth mechanism of gold nanorods (NRS) using Seed-Mediated growth method. *Chem Mater*. 2003;15(10):1957–1962.
14. Kim F, Song JH, Yang P. Photochemical synthesis of gold nanorods. *J Am Chem Soc*. 2002;124(48):14316–14317.
15. Tsuji M, Hashimoto M, Nishizawa Y, Kubokawa M, Tsuji T. Microwave-assisted synthesis of metallic nanostructures in solution. *Chemistry*. 2005;11(2):440–452.
16. Alkilany AM, Nagaria PK, Hexel CR, et al. Cellular uptake and cytotoxicity of gold nanorods: molecular origin of cytotoxicity and surface effects. *Small*. 2009;5(6):701–708.
17. Vigderman L, Khanal BP, Zubarev ER. Functional gold nanorods: synthesis, self-assembly, and sensing applications. *Adv Mater*. 2012;24(36):4811–4841.
18. Xie J, Lee S, Chen X. Nanoparticle-based theranostic agents. *Adv Drug Deliv Rev*. 2010;62(11):1064–1079.
19. Liu X, Huang N, Li H, et al. Multidentate polyethylene glycol modified gold nanorods for in vivo near-infrared photothermal cancer therapy. *ACS Appl Mater Interfaces*. 2014;6(8):5657–5668.
20. Alkilany AM, Thompson LB, Boulos SP, Sisco PN, Murphy CJ. Gold nanorods: their potential for photothermal therapeutics and drug delivery, tempered by the complexity of their biological interactions. *Adv Drug Deliv Rev*. 2012;64(2):190–199.
21. Xu L, Liu Y, Chen Z, et al. Surface-engineered gold nanorods: promising DNA vaccine adjuvant for HIV-1 treatment. *Nano Lett*. 2012;12(4):2003–2012.
22. Kah JC, Zubieta A, Saavedra RA, Hamad-Schifferli K. Stability of gold nanorods passivated with amphiphilic ligands. *Langmuir*. 2012;28(24):8834–8844.
23. Yang J, Shen D, Zhou L, et al. Mesoporous silica-coated plasmonic nanostructures for surface-enhanced Raman scattering detection and photothermal therapy. *Adv Healthc Mater*. 2014;3(10):1620–1628.
24. Wang L, Lin X, Wang J, et al. Novel insights into combating cancer chemotherapy resistance using a plasmonic nanocarrier: enhancing drug sensitiveness and accumulation simultaneously with localized mild photothermal stimulus of femtosecond pulsed laser. *Adv Funct Mater*. 2014;24(27):4229–4239.
25. Zhang Z, Wang L, Wang J, et al. Mesoporous silica-coated gold nanorods as a light-mediated multifunctional theranostic platform for cancer treatment. *Adv Mater*. 2012;24(11):1418–1423.
26. Li N, Niu D, Jia X, et al. Multiple gold nanorods@hierarchically porous silica nanospheres for efficient multi-drug delivery and photothermal therapy. *Journal of Materials Chemistry B*. 2017;5(8):1642–1649.
27. Ni Q, Teng Z, Dang M, et al. Gold nanorod embedded large-pore mesoporous organosilica nanospheres for gene and photothermal cooperative therapy of triple negative breast cancer. *Nanoscale*. 2017;9(4):1466–1474.
28. Lee C, Hwang HS, Lee S, et al. Rabies Virus-Inspired silica-coated gold nanorods as a photothermal therapeutic platform for treating brain tumors. *Adv Mater*. 2017;29(13):1605563.
29. Li C, Zhang Y, Li Z, et al. Light-responsive biodegradable Nanorattles for cancer theranostics. *Adv Mater*. 2018;30(8):1706150.
30. Kang Y, Taton TA. Core/Shell gold nanoparticles by self-assembly and crosslinking of micellar, block-copolymer shells. *Angew Chem Int Ed Engl*. 2005;44(3):409–412.
31. Niu D, Ma Z, Li Y, Shi J. Synthesis of core-shell structured dual-mesoporous silica spheres with tunable pore size and controllable shell thickness. *J Am Chem Soc*. 2010;132(43):15144–15147.

32. Chen O, Riedemann L, Etoc F, et al. Magneto-fluorescent core-shell supernanoparticles. *Nat Commun*. 2014;5:5093–5110.
33. Ma M, Zhang Y, Gong H, Li F, Gu N. Silica-coated magnetite nanoparticles labeled by nimotuzumab, a humanised monoclonal antibody to epidermal growth factor receptor: preparations, specific targeting and bioimaging. *J Nanosci Nanotechnol*. 2013;13(10):6541–6545.
34. Amoozgar Z, Yeo Y. Recent advances in stealth coating of nanoparticle drug delivery systems. *Wiley Interdiscip Rev Nanomed Nanobiotechnol*. 2012;4(2):219–233.
35. Wang J, Byrne JD, Napier ME, Desimone JM. More effective nanomedicines through particle design. *Small*. 2011;7(14):1919–1931.
36. Zhang Q, Wang X, Li PZ, et al. Cancer treatment: biocompatible, uniform, and Redispersible mesoporous silica nanoparticles for Cancer-Targeted drug delivery in vivo (AdV. Funct. mater. 17/2014). *Adv Funct Mater*. 2014;24(17):2450–2461.
37. Yin NQ, Wu P, Yang TH, Wang M. Preparation and study of a mesoporous silica-coated Fe_3O_4 photothermal nanoprobe. *RSC Advances*. 2017;7(15):9123–9129.
38. Lee KS, El-Sayed MA. Gold and silver nanoparticles in sensing and imaging: sensitivity of plasmon response to size, shape, and metal composition. *J Phys Chem B*. 2006;110(39):19220–19225.
39. Horiguchi Y, Honda K, Kato Y, Nakashima N, Niidome Y. Photothermal reshaping of gold nanorods depends on the passivating layers of the nanorod surfaces. *Langmuir*. 2008;24(20):12026–12031.
40. Ali MR, Rahman MA, Wu Y, et al. Efficacy, long-term toxicity, and mechanistic studies of gold nanorods photothermal therapy of cancer in xenograft mice. *Proc Natl Acad Sci U S A*. 2017;114(15):E3110–E3118.
41. Chon JWM, Bullen C, Zijlstra P, Gu M. Spectral encoding on gold nanorods doped in a silica Sol–Gel matrix and its application to high-density optical data storage. *Adv Funct Mater*. 2007;17(6):875–880.
42. Zijlstra P, Chon JW, Gu M. Effect of heat accumulation on the dynamic range of a gold nanorod doped polymer nanocomposite for optical laser writing and patterning. *Opt Express*. 2007;15(19):12151–12160.